

Extended damage range of $(Al_{0.3}Cr_{0.2}Fe_{0.2}Ni_{0.3})_3O_4$ high entropy oxide films induced by surface irradiation

Jian-Cong Zhang(张健聪), Sen Sun(孙森), Zhao-Ming Yang(杨朝明), Nan Qiu(裘南), Yuan Wang(汪渊)

Citation: Chin. Phys. B . 2020, 29(6): 066104 . **doi:** 10.1088/1674-1056/ab8374
Journal homepage: http://cpb.iphy.ac.cn; http://iopscience.iop.org/cpb

What follows is a list of articles you may be interested in

Defects and electrical properties in Al-implanted 4H-SiC after activation annealing

Yi-Dan Tang(汤益丹), Xin-Yu Liu(刘新宇), Zheng-Dong Zhou(周正东), Yun Bai(白云), Cheng-Zhan Li(李诚瞻)

Chin. Phys. B . 2019, 28(10): 106101 . **doi:** 10.1088/1674-1056/ab3cc2

Interaction of two symmetric monovacancy defects in graphene

Wen-Yan Xu(徐文焱), Li-Zhi Zhang(张礼智), Li Huang(黄立), Yan-De Que(阙炎德), Ye-Liang Wang(王业亮), Xiao Lin(林晓), Shi-Xuan Du(杜世萱)

Chin. Phys. B . 2019, 28(4): 046801 . **doi:** 10.1088/1674-1056/28/4/046801

Transient competition between photocatalysis and carrier recombination in TiO_2 nanotube film loaded with Au nanoparticles

Shao Zhu-Feng, Yang Yan-Qiang, Liu Shu-Tian, Wang Qiang

Chin. Phys. B . 2014, 23(9): 096105 . **doi:** 10.1088/1674-1056/23/9/096105

Transient competition between photocatalysis and carrier recombination in TiO_2 nanotube film loaded with Au nanoparticles

Shao Zhu-Feng, Yang Yan-Qiang, Liu Shu-Tian, Wang Qiang

Chin. Phys. B . 2014, 23(9): 096102 . **doi:** 10.1088/1674-1056/23/9/096102

Extended damage range of $(Al_{0.3}Cr_{0.2}Fe_{0.2}Ni_{0.3})_3O_4$ high entropy oxide films induced by surface irradiation*

Jian-Cong Zhang(张健聪)†, Sen Sun(孙森)†, Zhao-Ming Yang(杨朝明), Nan Qiu(裘南), and Yuan Wang(汪渊)‡

Key Laboratory of Radiation Physics and Technology, Ministry of Education, Institute of Nuclear Science and Technology, College of Physics, Sichuan University, Chengdu 610064, *China*

(Received 31 January 2020; revised manuscript received 9 March 2020; accepted manuscript online 26 March 2020)

Irradiation makes structural materials of nuclear reactors degraded and failed. However, the damage process of materials induced by irradiation is not fully elucidated, mostly because the charged particles only bombarded the surface of the materials (within a few microns). In this work, we investigated the effects of surface irradiation on the indirect irradiation region of the $(Al_{0.3}Cr_{0.2}Fe_{0.2}Ni_{0.3})_3O_4$ high entropy oxide (HEO) films in detail by plasma surface interaction. The results show that the damage induced by surface irradiation significantly extends to the indirect irradiation region of HEO film where the helium bubbles, dislocations, phase transformation, and the nickel oxide segregation were observed.

Keywords: high entropy oxide films, surface irradiation, radiation-induced segregation, vacancies, extended irradiation damage region

PACS: 61.72.jd, 68.35.Dv, 68.37.–d, 81.07.–b **DOI:** 10.1088/1674-1056/ab8374

1. Introduction

In irradiation environment of nuclear reactors, incident particles bombard the target atoms of the structural materials and cause cascade collisions, creating a cascade of point defects and clusters of these defects in the crystal lattice, which will significantly lead to surface morphology changes,[1] segregation and phase transformation,[2,3] hardening and embrittlement,[4] high temperature creep,[5] high temperature cavity swelling,[6] corrosion and stress corrosion cracking[7] of the bulk structural materials. In general, the depth of ion irradiation, which we call surface irradiation (SI) in this article, is relatively shallow (within a few microns),[6] so that the resulting direct damage region is located on the surface of the bulk materials. However, some near surface damages can over-time diffuse into the bulk and result in a relatively large damaged volume in indirect irradiation region (IIR), thus leading to the performance degradation and failure of bulk materials. Obviously, this is related to the profound later behaviors of the defects created by SI, because the defects can move to the deeper region of the bulk materials which is far beyond the direct irradiation region (DIR) under the diffusion mechanism.

For the new fast reactors or fusion reactors in the future, the materials will be exposed to harsh environment with higher temperature and higher irradiation dose for a long time.[8] The effect of defects created by SI on IIR of the materials will be enhanced. In this regard, it is necessary to investigate specifically the effect of SI on the IIR of the materials for further exploring irradiation damage mechanism of materials. However, the current researches mainly focused on the evolutions or effects of defects in the DIR of the materials,[9,10] because the effect of SI on the IIR is negligible at lower temperatures and irradiation fluences. Compared with conventional irradiation facilities, plasma surface interaction (PSI) facility with high ion flux (1.0×10^{18} cm^{-2}·s^{-1}) and high temperature is a good platform to investigate the effect of SI to the IIR of materials, because it makes the damage of IIR more significant under the SI.

Recently, high entropy oxide (HEO) have received a lot of attention, which not only inherits the advantages of high-entropy materials, such as excellent high-temperature stability, high strength and radiation resistance,[9,11,12] but also exhibits other excellent functional properties.[13–17] The 'cocktail effect', which refers to the composite properties of HEO not only come from the basic properties of elements by the mixture rule but also from the mutual interactions among all the elements and from the severe lattice distortion,[18] enables HEO to combine the advantages of their components, such a fact made us aware, HEO containing aluminum and chromium elements may have the potential tritium permeation resistance,[19,20] which may be candidates of tritium permeation barrier for future fusion reactors. Therefore, the study of HEO SI effects is of great significance for the application of HEO in new reactors.

In this study, $(Al_{0.3}Cr_{0.2}Fe_{0.2}Ni_{0.3})_3O_4$ HEO films were irradiated by a low-energy and high-fluence PSI facility. We observed significant helium bubbles and dislocations as well

*Project supported by the National Key Research and Development Program of China (Grant No. 2017YFB0405702) and the National Natural Science Foundation of China (Grant No. 11775150).

†These authors contributed equally to this work.

‡Corresponding author. E-mail: wyuan@scu.edu.cn

© 2020 Chinese Physical Society and IOP Publishing Ltd

as the resulting phase separation and segregation of nickel in the IIR of the irradiated HEO film. The results revealed that the remarkably enlarged damage region of the HEO film under the SI was mediated by vacancy diffusion.

2. Experimental

A radio frequency reactive magnetron sputtering system and an ultra-high vacuum sintering furnace were used to prepare $(Al_{0.3}Cr_{0.2}Fe_{0.2}Ni_{0.3})_3O_4$ HEO films on single crystal Si (100) substrates. The sputtering target is combined by several scalloped sectors including aluminum (Al), chromium (Cr), iron (Fe), and nickel (Ni) (99.995% in purity). The Si substrate was ultrasonically washed with alcohol, acetone, and deionized water about 5 minutes in that order. Before depositing the HEO films, a titanium buffer layer with a thickness of about 200 nm on the Si substrate was used to better combine the HEO films with the silicon substrates. Ar and O_2 were used as sputtering gas and reactive gas, respectively. The sputtering power was kept at 60 W during the deposition. Then, the as-deposited films were annealed at an annealing temperature of 873 K in an ultra-high vacuum sintering furnace at a basic pressure of lower than 2.0×10^{-4} Pa for 2 h to obtain pristine HEO films. Some of the pristine HEO films were irradiated using 80-eV He^+ with irradiation fluence of 6.0×10^{19} cm^{-2} and 1.8×10^{21} cm^{-2} under a 5-Pa helium atmosphere in a PSI facility (the depth of irradiation is less than 2 nm according to the SRIM). The corresponding irradiation temperature and irradiation time of these samples were about 873 K, 1 min, and 973 K, 30 min, respectively, where the ion flux was kept at 1.0×10^{18} $cm^{-2}\cdot s^{-1}$. The others were annealed at 973 K for 1 h and 1173 K for 1 h, respectively.

Grazing incidence (2.0°) x-ray diffraction (GIXRD, Philips X Pert Pro MPD DY129) was used to determine the crystal structure of the films by using a diffractometer with Cu–K_α radiation source. The effective absorption depth T of materials to x-rays can be calculated by $T = L\sin\alpha/\mu$, where L is experimental constant (about 0.13), α is incident angle, μ is line absorption coefficient. $\mu = (K\lambda^3Z^4)\cdot\rho$, where K is constant, λ is wavelength of x-ray, Z is the atomic number. In this study, α is 2°, Z_{HEO} is about 14 which has the same atomic number as Si, ρ_{HEO} is about 3.42 g$\cdot$ cm^{-3} calculated by SRIM, ρ_{Si} is about 2.33 g$\cdot$ cm^{-3}, $\mu_{Si} = 132$ cm^{-1},[21] $\mu_{HEO} = \mu_{Si}\cdot\rho_{HEO}/\rho_{Si} = 194$ cm^{-1}, thus $T_{HEO} = L\sin\alpha/\mu_{HEO} = 234$ nm. Since the SI depth is extremely shallow (less than 2 nm), which well below the depth sensitivity of XRD, it can be considered that the crystal structure information measured by XRD is mainly located in the IIR. A transmission electron microscope (TEM, Zeiss Libra200FE) and scanning transmission electron microscope (STEM, Zeiss Libra200FE) with an energy-dispersive spectrometer (EDS) operated at 200 keV was employed for the cross-sectional morphology, chemical compositions, and high angle annular dark field (HAADF) images of the HEO films. TEM foils of the samples were prepared by mechanical polishing to a thickness of approximately 50 μm, followed by Ar^+ ion milling (Leica EM RES101) to no more than 200 nm. In the process of ion milling, Ar^+ with 6-keV energy was first used to mill the samples at an angle of 6° for 2 hours, then Ar^+ with 3-keV energy was used to mill the samples at an angle of 3° until the samples were just perforated. The flux of Ar^+ were kept at 6.25×10^{13} $cm^{-2}\cdot s^{-1}$.

3. Results and discussion

3.1. Structure characterization of the HEO films

The GIXRD pattern in Fig. 1(a) and selected area electron diffraction (SAED) pattern in Fig. 1(b) show that the pristine film possesses a spinel structure. The high resolution transmission electron microscope (HRTEM) image (Fig. 1(c)) shows that the (111) plane spacing of the pristine film is 4.78 Å, in accordance with the XRD result. Meanwhile, the distribution of all the elements (Fig. 1(d)) is relatively uniform and the proportion of each metal element in the sample is 31% for Al, 20% for Cr, 18% for Fe, and 31% for Ni, respectively, in agreement with the concentration range of the principal element of the high entropy materials. These results reveal that the pristine samples are HEO films with spinel structure.

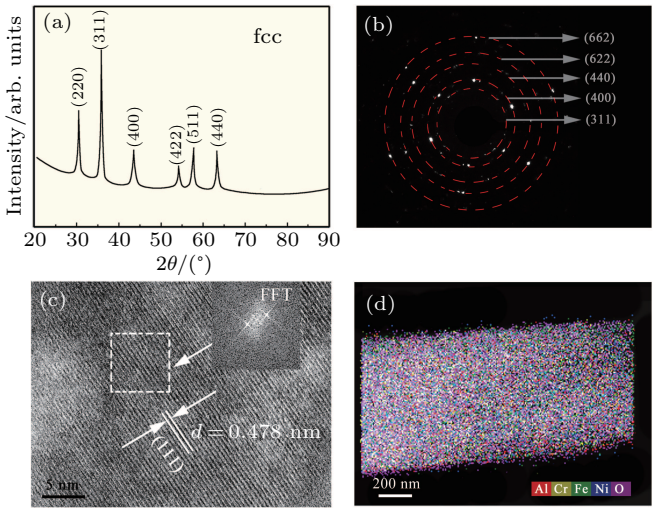


Fig. 1. Pristine HEO film: (a) GIXRD spectra, (b) selected area electron diffraction (SAED) image, (c) high resolution transmission electron microscope (HRTEM) image, (d) EDS-mapping image.

3.2. Phase transition of the HEO films induced by surface irradiation

Figure 2(a) shows the GIXRD patterns of the HEO films irradiated with different He^+ fluences. The pristine HEO film has a single spinel structure. However, a new phase with face-centered cubic (fcc_1) structure can be observed increasingly as the fluences of irradiation increased. Moreover, the full width at half maximum of the (311) peak increases obviously after irradiation at a fluence of 1.8×10^{21} cm^{-2}. These results

demonstrate that the crystal structure of HEO films are significantly broken down by SI.

Since the solid-state phase transformation can be induced either or both by ion irradiation and high temperature, in order to investigate whether irradiation or high temperature played an important role in the phase transformation of the irradiated samples, we performed high temperature annealing experiments as a control group. Figure 2(b) shows the evolution of the GIXRD patterns of the HEO films annealed at different temperatures. The spinel structure of the HEO films remain stable as the annealing temperature increased, and even after annealing at 1173 K which is higher than the irradiation temperature, indicating that the destruction of phase structures of the HEO films are induced by irradiation, although the depth of the SI of the HEO film is very shallow (less than 2 nm). The inset in Fig. 2(a) is the XRD peak angle changes of crystal plane (400) of the irradiated films at different irradiation fluences. The result shows that the diffraction peaks of the irradiated HEO films shift slightly to higher angle as the irradiation fluence increases, while no diffraction peaks shifting could be found in the annealed HEO films in Fig. 2(b). This is becuse the lattice atoms of the irradiated HEO films are squeezed by the helium clusters or bubbles,[22,23] which was confirmed in the analysis later of this paper.

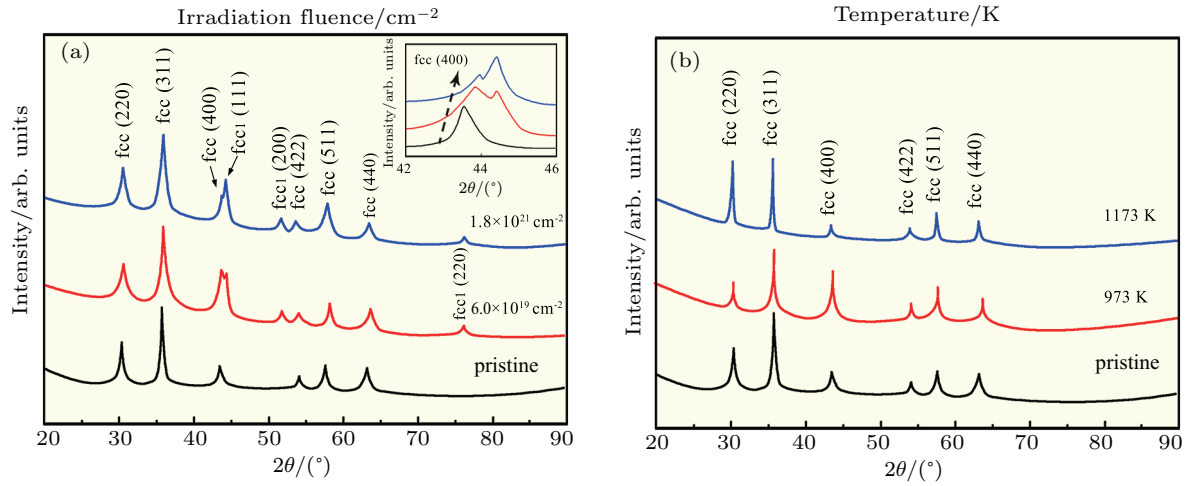


Fig. 2. GIXRD patterns of the HEO films: (a) the films exposed to different irradiation fluences, (b) the films annealed at different temperatures.

3.3. Defect evolution of the HEO films induced by surface irradiation

The cross-section TEM image of the irradiated HEO film at a fluence of 1.8×10^{21} cm^{-2} is shown in Fig. 3(a). It can be clearly found that a large number of helium bubbles were aggregated in a vertical strip shape (marked by white arrows) along the columnar grain boundaries of the irradiated HEO film. However, no helium bubbles were found along the columnar grain boundaries (marked by white arrows in Fig. 3(d)) of the pristine HEO film. Since the helium bubbles are combinations of helium atoms and vacancies,[22] it indicates that the vacancies created by SI (less than 2 nm) have diffused through the grain boundaries and grains to the IIR of the HEO film, which have greatly extended the damage range of the HEO film.

Moreover, the helium bubbles near the surface of the irradiated HEO film exhibit smaller size and higher density platelet distribution (marked by red ellipses and inset A in Fig. 3(a)). One of the effects, which could be responsible for smaller voids near the surface compared to the "bulk" voids, is that the surface acts as a sink for helium, and this cannot stabilize (radiation-induced or thermal) vacancies. Thus, the resulting cavities are smaller. However, near the bottom of the irradiated HEO film, larger-size and lower-density helium bubbles are distributed along the grain boundaries in the variety form of irregular polyhedrons (marked by blue ellipse and inset B in Fig. 3(a)). It indicating that the intragranular vacancies or voids were attracted and combined by the grain boundaries to form larger voids during downward diffusion.

It is necessary to point out that such large and dense helium bubbles in IIR of the HEO film was induced by SI rather than ion milling. Although vacancies may be created by Ar^+ bombardment during ion milling, the irradiation flux of Ar^+ are four orders of magnitude lower than that of He^+, so that the dpa produced by Ar^+ is three orders of magnitude lower than that by He^+. Moreover, the ion milling temperature is significantly lower than the SI temperature, which is not conducive to the growth of the vacancies. Therefore, no visible cavities/voids were found in the pristine HEO film (Fig. 3(d)) which was only ion milled without SI.

Figures 3(b) and 3(c) show the HRTEM images of the irradiated HEO film. It can be seen that the helium bubbles were trapped on the grain boundaries (Fig. 3(b)) which have lower potential energies. Many Moire fringes appeared around the helium bubbles (marked by white ellipses in Fig. 3(b)) or even far away from the helium bubbles (Fig. 3(c)), but no sim-

ilar scenario appeared in the HRTEM image of the pristine HEO film (Fig. 3(e)), indicating that helium bubbles originating from the SI exerted a significant compressive stress to the IIR of the irradiated HEO film, which confirmed that the shift of the XRD peaks (the inset of Fig. 2(a)) is from the squeeze of the helium pressure in the He–vacancy clusters/bubbles. Moreover, in the inverse fast Fourier transform (IFFT, Fig. 3(f)), a large number of dislocations and lattice distortions can be found, indicating that new defects in IIR of the HEO film were created under the effect of helium bubbles.

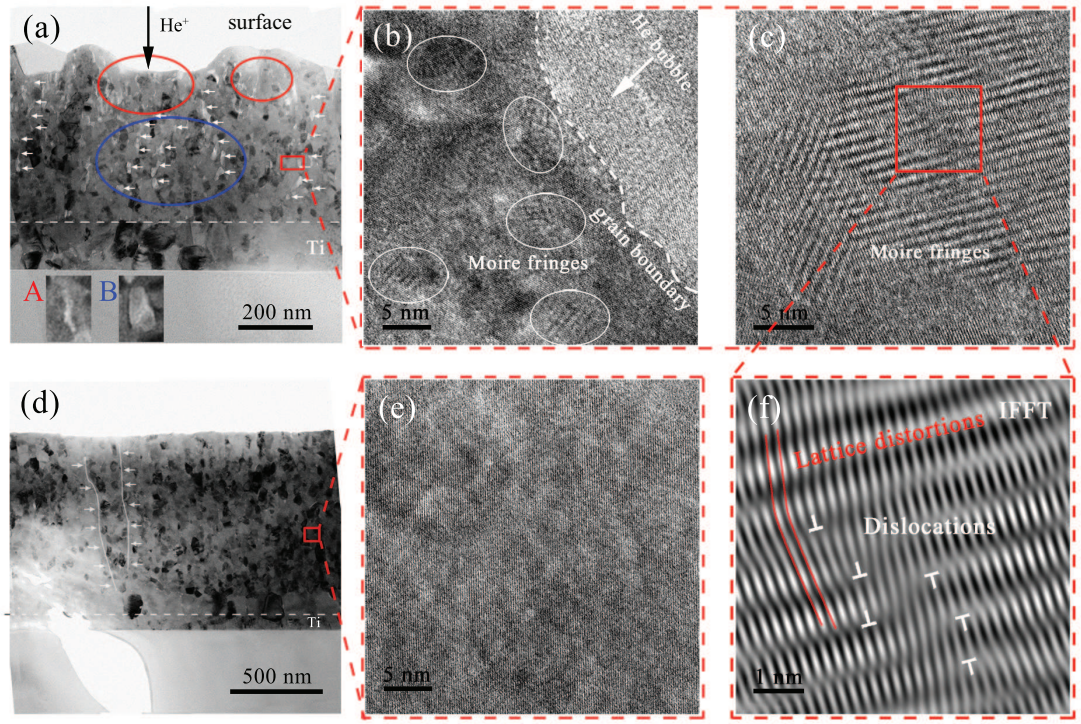


Fig. 3. Cross-sectional TEM image (a), HRTEM image [(b) and (c)], and the inverse fast Fourier transform (IFFT) image (f) of the irradiated HEO film at an fluence of 1.8×10^{21} cm^{-2}. Cross-sectional TEM (d) and HRTEM (e) images of the pristine HEO film.

3.4. Element segregation of the HEO films induced by surface irradiation

The cross-section HAADF and EDS-mapping images of the irradiated HEO film is shown in Fig. 4. Some strips stacked with white spots, which are almost vertically distributed in/run through the film, were observed in Fig. 4(a) (marked by white arrows). Moreover, a remarkable enrichment and depletion area of the Ni element in the IIR (marked by white arrows in Fig. 4(b)) was observed in the same position of the HAADF image (Fig. 4(a)) of the irradiated HEO film, which is consistent with the new phase structure of fcc_1 in XRD results. However, the distribution (Fig. 1(d)) of all the elements in pristine HEO film is uniform. It indicates that SI induced significant element segregation in IIR of the irradiated HEO film.

It is clear from the above-mentioned discussion that the radiation-induced segregation (RIS) of Ni is closely related to the helium bubbles behavior as shown in Figs. 3(a) and 4(a). It is known that RIS is an enhanced diffusion of elements of materials under the effect of point defects (vacancies and interstitials) with low migration energy, leading to enrichment or depletion of the elements near sinks of the irradiated materials. In this study, the RIS is dominated by vacancy exchange mechanism,[2] and the shape and distribution of helium bubbles can reveal the vacancy diffusion behaviors. Therefore, we can infer that due to the attraction of the columnar grain boundaries of the HEO film, the intragranular He–vacancy complexes diffuse to the grain boundaries and then accumulate and combined into helium bubbles with strip distribution. Meanwhile the elements diffuse in the opposite direction, forming the enrichment and depletion near the grain boundaries.

Interestingly, only Ni element exhibits visible segregation while no segregation of other elements was observed in Fig. 4, suggesting that Ni element has the largest diffusion coefficient and preferentially exchanges with vacancies of the HEO film. In general, the diffusion coefficient of elements depends on their activation energy, which is dominated by their electronegativity for ionic compounds.[3,24,25] The smaller the electronegativity difference between anions and cations, the smaller the diffusion activation energy of ions. As shown in Table 1, the electronegativity difference between nickel and oxygen is the smallest among the electronegativity differences of all metal cations and oxygen anions, thus the diffusion coefficient of nickel is the largest and the exchange interplay between nickel ions and vacancies is the strongest in all cations, which is consistent with the experimental result that only nickel exhibited significant segregation in the irradiated HEO film.

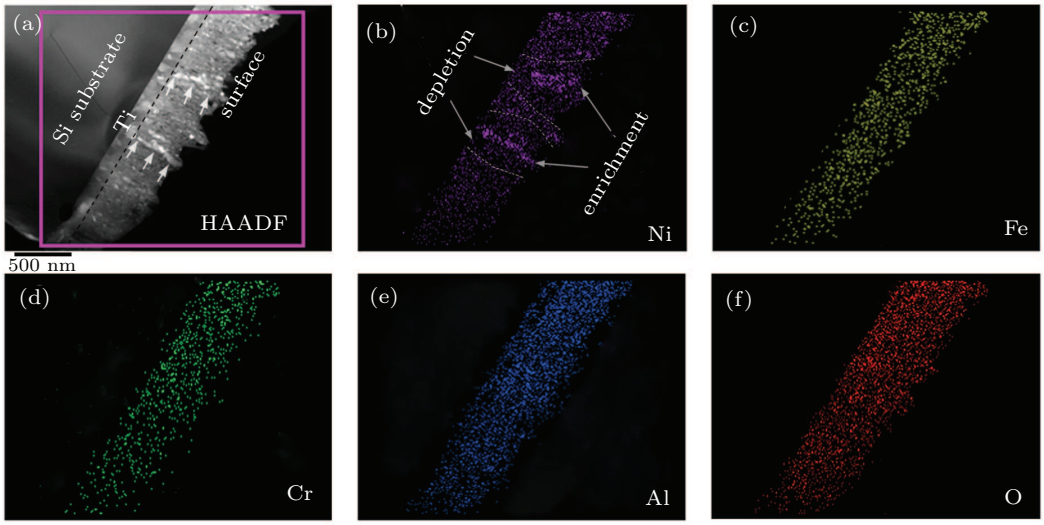


Fig. 4. HAADF image (a) and EDS-mapping images of Ni (b), Fe (c), Cr (d), Al (e), and O (f) of the irradiated HEO films with an irradiation fluence of 1.8×10^{21} cm^{-2}.

Table 1. Electronegativity of all relevant elements.[26]

Elements	O	Al	Cr	Fe	Ni
Electronegativity	3.44	1.61	1.66	1.83	1.91

4. Conclusions

In summary, we have successfully prepared HEO films by magnetron sputtering incorporating with post annealing, and investigated the microstructure changes of IIR of the HEO films induced by SI in details. The results show the microstructure damages induced by SI far exceeded the DIR, leading to significant helium bubble aggregation, segregation of nickel, and phase separation throughout the HEO film. Further analysis revealed that the diffusion of the He–vacancy complex plays a major role in the extended damage range of ion irradiation due to the stabilizing effect of helium on the vacancies. This gives us a definitive proof that although the DIR of the ion irradiation is limited to the surface of materials, the mediation of the He–vacancy complex diffusion will significantly extend the damage region of the materials, especially for new generation advanced reactors, accelerating the degradation and failure of structure or performance of materials, and thus shorten the service time of materials in the nuclear reactor. Therefore, reducing the helium content in the radiation through some appropriate methods may be an effective approach to design radiation-tolerance materials.

References

[1] Tripathi J K, Novakowski T J and Hassanein A 2016 *Appl. Surf. Sci.* **378** 63
[2] Sun S, Qiu N, Zhang K, He P N, Ma Y J, Gou F J and Wang Y 2019 *Scr. Mater.* **161** 40
[3] Xia S Q, Gao M C, Yang T F, Liaw P K and Zhang Y 2016 *J. Nucl. Mater.* **480** 100
[4] Xiao X 2019 *Metals* **9** 1132
[5] Bufford D C, Barr C M, Wang B M, Hattar K and Haque A 2019 *JOM* **71** 3350
[6] Was G S 2015 *Fundamentals of Radiation Materials Science*, 2nd edn. (Ann Arbor, MI: Springer) pp. 167–199
[7] Kuang W, Hesterberg J and Was G S 2019 *Corros. Sci.* **161** 108183
[8] Zinkle S J and Was G S 2013 *Acta Mater.* **61** 735
[9] Lu C Y, Niu L L, Chen N J, Jin K, Yang T N, Xiu P Y, Zhang Y W, Gao F, Bei H B, Shi S, He M R, Robertson I M, Weber W J and Wang L M 2016 *Nat. Commun.* **7** 13564
[10] Wei Y X, Shen Z Y, Zhang W P, Tang R, Long Y X, Chen C, Zhou X, Guo L P and Qiu S 2019 *Nucl. Instrum. Methods Phys. Res. Sect. B* **459** 7
[11] Rost C M, Sachet E, Borman T, Moballegh A, Dickey E C, Hou D and Jones J L 2015 *Nat. Commun.* **6** 8485
[12] Kumar N A P K, Li C, Leonard K J, Bei H and Zinkle S J 2016 *Acta Mater.* **113** 230
[13] Bérardan D, Franger S, Dragoe D, Meena A K and Dragoe N 2016 *Phys. Status Solidi-Rapid Res. Lett.* **10** 328
[14] Bérardan D, Franger S, Meena A K and Dragoe N 2016 *J. Mater. Chem. A* **4** 9536
[15] Qiu N, Chen H, Yang Z M, Sun S, Wang Y and Cui Y H 2019 *J. Alloys Compd.* **777** 767
[16] Braun J L, Rost C M, Lim M, Giri A, Olson D H, Kotsonis G N, Stan G, Brenner D W, Maria J P and Hopkins P E 2018 *Adv. Mater.* **30** 1805004
[17] Yang Z M, Zhang K, Qiu N, Zhang H B, Wang Y and Chen J 2019 *Chin. Phys. B* **28** 046201
[18] Gao M C, Yeh J W, Liaw P K and Zhang Y 2016 *High-Entropy Alloys, Fundamentals and Applications* (Switzerland: Springer International Publishing) pp. 62–64
[19] Tsai M and Yeh J W 2014 *Mater. Res. Lett.* **2** 107
[20] Zheng G, Carpenter D, Dolan K and Hu L 2019 *Nucl. Eng.* **353** 110232
[21] Lawrence J L 1977 *Acta Cryst. A* **33** 343
[22] Lao Y X, Niu W X, Shi Y L, Du H, Zhang H B, Hu S L and Wang Y 2018 *J. Alloys Compd.* **739** 401
[23] Garner F A and Toloczko M B 1997 *J. Nucl. Mater.* **251** 252
[24] Egami T, Ojha M, Khorgolkhuuk O, Nicholson D M and Stocks G M 2015 *JOM* **67** 2345
[25] Tsai K Y, Tsai M H and Yeh J W 2013 *Acta Mater.* **61** 4887
[26] Nie C M, Wen S N, Li Z H, Xie S B and Wang H Q 2002 *Acta Chim. Sin.* **60** 207